Published in final edited form as:
J Comp Neurol. 2010 November 1; 518(21): 4463–4478. doi:10.1002/cne.22467.

EVIDENCE OF CELL-NONAUTONOMOUS CHANGES IN DENDRITE AND DENDRITIC SPINE MORPHOLOGY IN THE MET-SIGNALING DEFICIENT MOUSE FOREBRAIN

Matthew C. Judson[3,*], **Kathie L. Eagleson**[5], **Lily Wang**[1,4], and **Pat Levitt**[1,2,5]

[1] Vanderbilt Kennedy Center for Research on Human Development, Vanderbilt University Medical Center, Nashville, TN 37203

[2] Department of Pharmacology, Vanderbilt University Medical Center, Nashville, TN 37203

[3] Graduate Program in Neuroscience, Vanderbilt University Medical Center, Nashville, TN 37203

[4] Department of Biostatistics, Vanderbilt University Medical Center, Nashville, TN 37203

[5] Zilkha Neurogenetic Institute and the Department of Cell and Neurobiology, Keck School of Medicine, University of Southern California, Los Angeles, CA 90089

Abstract

Human genetic findings and murine neuroanatomical expression mapping have intersected to implicate Met receptor tyrosine kinase signaling in the development of forebrain circuits controlling social and emotional behaviors that are atypical in autism spectrum disorders (ASD). To clarify roles for Met signaling during forebrain circuit development *in vivo*, we generated mutant mice ($Emx1^{Cre}/Met^{fx/fx}$) with an Emx1-Cre-driven deletion of signaling-competent Met in dorsal pallially-derived forebrain neurons. Morphometric analyses of Lucifer Yellow-injected pyramidal neurons in postnatal day 40 anterior cingulate cortex (ACC) revealed no statistically significant changes in total dendritic length, but a selective reduction in apical arbor length distal to the soma in $Emx1^{Cre}/Met^{fx/fx}$ neurons relative to wild type, consistent with a decrease in the total tissue volume sampled by individual arbors in the cortex. The effects on dendritic structure appear to be circuit-selective, as basal arbor length was *increased* in $Emx1^{Cre}/Met^{fx/fx}$ layer 2/3 neurons. Spine number was not altered on $Emx1^{Cre}/Met^{fx/fx}$ pyramidal cell populations studied, but spine head volume was significantly increased (~20%). Cell-nonautonomous, circuit-level influences of Met signaling on dendritic development were confirmed by studies of medium spiny neurons (MSN), which do not express Met, but receive Met-expressing corticostriatal afferents during development. $Emx1^{Cre}/Met^{fx/fx}$ MSN exhibited robust increases in total arbor length (~20%). Like in the neocortex, average spine head volume was also increased (~12%). These data demonstrate that a developmental loss of presynaptic Met receptor signaling can affect postsynaptic morphogenesis and suggest a mechanism whereby attenuated Met signaling could disrupt both local and long-range connectivity within circuits relevant to ASD.

Introduction

The α,β-heterodimeric, transmembrane Met receptor tyrosine kinase binds its endogenous ligand, hepatocyte growth factor (HGF), and signals to promote a variety of developmental processes in epithelially-derived tissues. At the single-cell level these include cell

Correspondence to: Pat Levitt, Ph.D., Director, Zilkha Neurogenetic Institute, Chair, Dept. Cell and Neurobiology, Keck School of Medicine of USC, 1501 San Pablo Street, Los Angeles, CA 90089-2821, plevitt@usc.edu, 323-442-1509, 323-442-2145, (fax) www.usc.edu/zni.

proliferation, migration, differentiation, and survival (Ebens et al., 1996; Hamanoue et al., 1996; Caton et al., 2000; Ieraci et al., 2002; Gutierrez et al., 2004; Giacobini et al., 2007; Garzotto et al., 2008; Lim and Walikonis, 2008). HGF-Met signaling also plays a critical role in higher-order developmental processes such as epithelial tubulugenesis and duct formation, which requires the organization of complex interactions among many polarized cells (Rosario and Birchmeier, 2003; Zhang and Vande Woude, 2003).

Circuit wiring and synaptogenesis in the nervous system also require the exquisite control and coordination of interactions among polarized cells. Recent evidence indicates that HGF-Met signaling may help regulate these processes within specific circuits of the mammalian forebrain. Met expression mapping during the period of forebrain wiring and synaptogenesis reveals a striking enrichment of the receptor in the neuropil and long-projecting axons of the cerebral cortex, hippocampus and amygdala, suggesting that disrupted Met signaling could result in aberrant connectivity between these structures (Judson et al., 2009). Such a disruption would be predicted to impact the function of circuits governing social and emotional dimensions of behavior, consistent with recent genetic findings from ours and two other laboratories that two different alleles of the human *MET* gene are associated with autism spectrum disorders (ASD) (Campbell et al., 2006; Campbell et al., 2008; Jackson et al., 2009; Sousa et al., 2009). One variant reduces transcriptional efficiency, consistent with the reported 2-fold decrease in neocortical MET protein expression in ASD postmortem cases (Campbell et al., 2007). Moreover, further family-based analyses have revealed an enriched association of this same promoter variant with social and communication phenotypes of ASD (Campbell et al., 2009).

There are a number of studies of neurons in vitro that demonstrate the importance of Met signaling for neuronal differentiation and synapse organization (Powell et al., 2003; Gutierrez et al., 2004; Madhavan and Peng, 2006; Tyndall and Walikonis, 2006; Nakano et al., 2007; David et al., 2008; Lim and Walikonis, 2008). However, despite these converging lines of evidence supporting a role for Met signaling in the proper wiring of circuits which in human may be vulnerable in ASD, precisely *how* disrupted Met signaling might affect *in vivo* circuit development has yet to be addressed experimentally. In the present study, we applied our neuroanatomically-based understanding of developmental forebrain Met expression to the study of dendritic morphology in neurons from wild type mice and conditional mutant mice in which Met receptors are functionally deleted in forebrain structures originating from the dorsal pallium. Specifically, we describe the dendritic morphometry of Lucifer Yellow-injected wild type and mutant projection neurons in both the anterior cingulate cortex (ACC) and the dorsolateral striatum. ACC pyramidal neurons are of interest due to their important roles in limbic circuit function and the shared expression of Met in these cells in mouse and primate cortex (M. Judson, D. Amaral, P. Levitt, unpublished observations). To address possible non-cell autonomous effects of deleting Met, we examined medium spiny neurons (MSN) of the dorsolateral striatum. These neurons do not express Met transcript or protein, but receive abundant Met-expressing corticostriatal afferents during development (Judson et al., 2009).

Materials and Methods

Breeding and genotyping mice

Conditional Met mutant mice ($Emx1^{Cre}/Met^{fx/fx}$) were generated and genotyped using previously described strategies (Judson et al., 2009). Briefly, homozygous Met floxed ($Met^{fx/fx}$) mice were crossed to heterozygous Emx1-Cre knock-in mice that were also heterozygous for the floxed *Met* allele ($Emx1^{Cre}/Met^{fx/+}$). All resultant progeny were genotyped by polymerase chain reaction (PCR) using the following PCR primer sets: *$Emx1^{Cre}$ forward 5_-TTCGGCTATACGTAACAGGG-3_ and reverse 5_-*

*TCGATGCAACGAGTGATGAG-3_; Met^{fx} forward 5_-GCAACTGTCTTTTGATCCCTGC-3_ and reverse 5_TGTCCAGCAAAGTCCCATGATAG-3_*. Met^{fx} (Courtesy of Dr. Snorri Thorgeirsson, NIH/Center for Cancer Research, Bethesda, MD) and Emx1^{Cre} breeding lines (courtesy of Dr. Kevin Jones, University of Colorado, Boulder, CO) were backcrossed onto the C57BL/6J background for greater than 10 generations. Emx1^{Cre} mice show spatiotemporal patterns of Cre recombinase expression like those observed for endogenous Emx1 (Gorski et al., 2002). All research procedures using mice were approved by the Institutional Animal Care and Use Committee at Vanderbilt University and conformed to NIH guidelines. All efforts were made to minimize animal suffering and to reduce the number of animals used.

Antibody characterization

Please see Table 1 for a list of all antibodies used.

Both Met antisera recognized only the expected precursor (170 kD) and processed (140 kD) bands on Western blots of wild type mouse cortical lysate. Recognition of the 140 kD band was drastically reduced on Western blots of Emx1^{Cre}/Met$^{fx/fx}$ cortical lysate (Judson et al., 2009; **data not shown**).

The phosphorylated Met antiserum recognized a single band of 140 kD on Western blots of wild type but not Emx1^{Cre}/Met$^{fx/fx}$ mouse cortical synaptosomes stimulated with HGF. Furthermore, this antiserum stained the axon terminals of forebrain projection neurons in fixed brain sections from P7 wild type mice (**data not shown**). No staining was observed in brain sections from Emx1^{Cre}/Met$^{fx/fx}$ mice of the same age.

Antiserum against lucifer yellow stained only forebrain neurons in which lucifer yellow dye had been injected intracellularly (see Figs 2A,3A,6A). Brain regions in which no injections were made were completely devoid of staining.

Immunoprecipitation

Postnatal day 7 (P7) mice were deeply anesthetized with isofluorane prior to decapitation and brain removal. Each brain was immediately immersed in room temperature Hanks' balanced salt solution (Sigma, St. Louis, MO), and the cerebral cortex was rapidly dissected from each hemisphere with the aid of an MZ-6 stereozoom microscope (Leica, Bannockburn, IL). Harvested cerebral cortices were immediately snap-frozen in liquid nitrogen and stored at −80°C to await immunoprecipitation (IP) analysis.

Lysates for IP were prepared by homogenizing frozen P7 cerebral cortices in a glass tissue homogenizer (Wheaton, Millville, NJ) with ice-cold IP buffer (50 mM Tris HCl, pH 8.0, 150 mM NaCl, 1% Nonidet P-40) containing a protease inhibitor cocktail (Sigma), both serine/threonine and tyrosine phosphatase inhibitor cocktails (Sigma), 10 mM activated Na3VO4, 1mM EDTA, and 1mM EGTA. The lysates were cleared by a 16,000*g* centrifugation for 20 minutes at 4°C, and protein concentrations of the supernatants were determined using the Dc protein assay (Bio-Rad, Hercules, CA). Wild type and Emx1^{Cre}/Met$^{fx/fx}$ cortical lysates were diluted to a concentration of 2 mg/ml with IP buffer, and 1ml of 2 mg/ml lysate was incubated for 12 hours at 4°C with 75 μl of either mouse anti-Met (Cell Signaling #3127) or nonimmunized mouse IgG (Jackson immunoresearch #015000003, West Grove, PA) linked to magnetic beads. Each IP antibody was covalently linked to magnetic M-280 Tosylactivated Dynabeads (Invitrogen, Carlsbad, CA) as per manufacturer's instructions. Subsequently, the IP beads were pelleted with the application of a magnetic field, and washed 3 times for 5 minutes each at 4°C in phosphate-buffered saline (PBS), pH 7.5, containing protease and phosphatase inhibitors and 0.005% Nonidet P-40 detergent. The washed IP beads were then resuspended in 60 ul of Laemmli buffer containing 5% 2-

Mercaptoethanol and incubated at 75°C for 5 minutes to elute the IP complexes. IP eluates were stored at −20C prior to SDS-PAGE and Western blotting.

HGF stimulation of cortical synaptosomes

Frozen cortices from P7 wild type and $Emx1^{Cre}/Met^{fx/fx}$ mice were thawed in ice-cold fractionation buffer (320 mM sucrose in 7mM Tris-HCL, pH 7.5, containing protease inhibitors (Sigma)) and then fractionated using a glass tissue homogenizer (Wheaton). One ml of fractionation buffer per whole cortex was used. The fractionated samples were then centrifuged at 4°C at 900*g* for 15 minutes to pellet nuclei and blood vessels. The nuclear pellets were discarded and the supernatants were further centrifuged at 14,500*g* for 15 minutes to yield pellets containing crude cell membranes and synaptosomes. Each crude synaptosomal pellet was then resuspended in ice-cold artificial cerebral spinal fluid (12.4 mM NaCl, 0.4 mM KCl, 0.1 mM KH_2PO_4, 0.25 mM $CaCl_2$, 0.1 mM $MgCl_2$, 1 mM dextrose, and 2.6 mM $NaHCO_3$), freshly bubbled with 95% O_2/5% CO_2. At this stage, human recombinant HGF (R&D Systems, Minneapolis, MN) was added to some of the resuspended synaptosomes at a final concentration of 50 ng/ml to stimulate Met receptor phosphorylation. After a 5 minute incubation on ice, both stimulated and unstimulated synaptosomes were centrifuged at 14,500*g* for 15 minutes at 4°C, and the resulting pellets were lysed with 100 μl of IP buffer and vigorous mixing. Synaptosomal lysates were cleared by a 16,000*g* centrifugation for 20 minutes at 4°C, and protein concentrations of the supernatants were determined using the Dc protein assay (Bio-Rad). Samples were stored at −80°C prior to SDS-PAGE and Western blotting.

Western blotting

Protein samples (15 μl of IP eluate per lane or 20μg synaptosomal protein per lane) were fractionated by SDS-PAGE and transferred to supported nitrocellulose membranes. Western blotting was then performed as described previously (Judson et al., 2009), using the primary antibody dilutions listed in Table 1: rabbit anti-phosphorylated Met and mouse anti-phosphorylated tyrosine were diluted in Blotto (3% Carnation dried milk in PBS) containing 0.1% Tween-20; mouse anti-Met (Santa Cruz #sc-8057) was diluted in Blotto alone. Anti-mouse and anti-rabbit horseradish peroxidase-conjugated secondary antibodies (Jackson Immunoresearch) were diluted to 1:5,000 with the same diluent as the primary antibody.

Intracellular injections, lucifer yellow immunohistochemistry, and morphometric reconstructions

A total of 11 P39-41 male mice (7 wild type and 4 $Emx1^{Cre}/Met^{fx/fx}$) were deeply anesthetized with sodium pentobarbital (60 mg/kg i.p.) prior to transcardial perfusion. To clear blood from the vasculature and facilitate more efficient tissue fixation, mice were first perfused with ~10mls of 37°C PBS, which was immediately followed by ~100 mls of room-temperature phosphate-buffered 4% paraformaldehyde (pH 7.3). Each fixed brain was then removed from the skull and post-fixed for 2 hours at 4°C before being sectioned coronally at a thickness of 200 μM with a vibratome (Vibratome, Saint Louis, MO). Fixed vibratome sections were then post-fixed for an additional 2 hours at 4°C before being rinsed and stored in cold PBS. Sections were stored in PBS at 4°C for up to 5 days prior to intracellular injections of Lucifer Yellow dye. Equivalent intervals between post-fixation and intracellular injection were maintained across animals for each anatomical region of interest.

The cell bodies of layer 5 and layer 2/3 pyramidal neurons in anterior cingulate cortex (at the level of the genu of the corpus callosum) and medium spiny neurons in dorsolateral striatum (at the level of the body of the anterior commissure) were targeted for injection with the aid of an Axioskop2 microscope and 40x immersion objective (Zeiss, Jena, Germany). The injected cells were within 3 focal planes of the upper surface of the brain

section and evenly spaced from previously injected cells. Then, a glass micropipette containing Lucifer Yellow dye (8% in 0.05 M Tris buffer, pH 7.4) was gently inserted into each targeted cell body using a micromanipulator, and a continuous current (5–15 nA) was applied until the tips of the most distal dendrites were brightly fluorescent.

Lucifer Yellow immunohistochemistry was used to yield a more photostable product within injected cells. Briefly, sections containing injected cells were placed in a stock solution (2% bovine serum albumin, 1% Triton X-100, and 5% sucrose in PBS) containing anti-Lucifer Yellow antibodies. Sections were incubated in the primary antibody solution at 4°C for 3–4 days before being rinsed several times in stock solution and incubated 2 hours at room-temperature in biotinylated anti-rabbit secondary antibody (RPN1004; GE/Amersham, Pittsburgh, PA). Several rinses in PBS followed, and sections were subjected to a final 2 hour room-temperature incubation in Alexa Fluor 488-conjugated streptavidin (Invitrogen) diluted 1:1,000 in PBS. After several more rinses in PBS, sections were mounted on uncoated glass slides and coverslipped with ProLong Gold mounting medium (Invitrogen).

An Olympus microscope with a motorized stage and Neurolucida software (Microbrightfield, Williston, VT) were used to three-dimensionally reconstruct the dendritic arbors of neurons whose dendrites were completely filled to the distal tips. Gross dendritic measures included primary dendrite number, total dendritic length, apical and basal dendritic length, average dendritic segment length, apical and basal average dendritic segment length, and three-dimensional (3D) convex hull volume. Sholl analyses (Sholl, 1953) were performed in order to detect regional changes in dendritic tree morphology. We performed Sholl analyses of dendritic length, branching complexity and branch node frequency on the entire dendritic arbors of all neurons sampled, as well as on the isolated basal and apical compartments of each pyramidal neuron.

Dendrites were frequently transected by the coronal plane of section, which severely limited the study of pyramidal apical dendritic arbors whenever the primary apical dendrite was cut off proximal to the cell body. Therefore, we chose to only analyze the arbors of layer 5 and layer 2/3 pyramidal cells with total apical dendritic lengths at least half that of their respective genotypic means. Seven wild type (3 layer 5 and 4 layer 2/3) and 6 $Emx1^{Cre/Met^{fx/fx}}$ (5 layer 2/3 and 1 layer 5) pyramidal cells were excluded from analysis based on this criterion. Between 3 and 6 cells per anatomical region per animal were included in the final analyses. Investigators were blind to the genotypic identities of the samples from the time of animal perfusion through the morphometric analysis of dendritic arbor structure.

Confocal microscopy and semi-automated analysis of dendritic spines

Using an approach based on previously described methods (Shen et al., 2008), dendrites of the same neurons subjected to Neurolucida analyses were imaged by confocal microscopy, and 3D renderings of the images were used to facilitate semi-automated quantification of dendritic spine density and dendritic spine head volume. Usually 2, but occasionally 1 or 3, dendritic segments located 60–120 μM (2^{nd}, 3^{rd}, or 4^{th} order) from the cell body were analyzed per cell. Briefly, a Zeiss LSM 510 confocal microscope (Zeiss, Jena, Germany) with 63x oil immersion objective, 4x digital cropping, and a frame size of 1024 × 1024 pixels was used to capture high-resolution images of dendritic segments with 0.035 μM × 0.035 μM pixel dimensions. Segments were scanned at 0.38 μM intervals along the Z axis.

Confocal images of dendritic segments were viewed using Imaris software (Version 6.3–64 bit, Bitplane, Saint Paul, MN) in the Surpass view. The Filament module (Autopath, no loops), was then used to generate a 3D segmented rendering of each dendritic segment that was between 30 μM and 35 μM in length on average. The minimum end-point diameter (smallest detected spine head) was set at 0.143 μM, and the fluorescence contrast threshold

was set ≥ to 3. Renderings were subsequently edited for accuracy relative to the actual confocal image, and data concerning spine density and end-segment diameter were exported to Microsoft Excel 2003 (Microsoft Incorporated, Redmond, WA) for summary statistical analyses. Investigators were unaware of sample genotypes both during the imaging and 3D rendering of dendritic segments.

Digital illustrations

Optical fluorescence microscopy was performed with the aid of an Axioplan II microscope (Zeiss), and low-power micrographs depicting fields of Lucifer Yellow-injected neurons were acquired with a Zeiss AxioCam HRc camera (Zeiss) in Axiovision 4.1 software (Zeiss). Alterations to contrast levels in these low-power images were performed using Adobe Photoshop (Version 7.0, Adobe, San Jose, CA). Figures were prepared digitally in Microsoft Office Powerpoint 2003 (Microsoft Incorporated).

Statistical analyses

All morphological data in the present study are summarized as means±SEM. Genotypic group differences in gross dendritic structure (e.g., total dendritic length and dendritic arbor volume) and all spine parameters were assessed using the two-sample, two-tailed t-test within GraphPad Prism (Version 4.0, GraphPad Software, La Jolla, CA), the software program used for the production of all data graphs. P-values less than 0.05 were considered significant. We applied a rigorous statistical Bonferroni correction for multiple comparisons of the distribution of spine head volume frequency.

Sholl analysis data, which describe changes in dendritic structure that occur as a function of radial distance from a neuronal cell body (Sholl, 1953), were analyzed within SAS (version 9.1.3, SAS institute, Cary, NC) Procedure GLIMMIX. Specifically, genotypic group differences within each anatomical region of interest were analyzed using a linear mixed model with dendritic length as the outcome, fixed group effects, radius, group × radius interaction, and random animal effects. The random animal effects, along with an autoregressive covariance structure for each neuron within an animal, account for correlations of repeated measurements from the same animal. Because both fixed and random effects are included, this model is a mixed effects model. To compare dendritic length at each radius for the two groups, parameters from the mixed model were estimated and compared. We used the Kenward-Roger's adjusted degrees of freedom solution (option DDFM=KR in Procedure GLIMMIX) for statistical inference (Kenward and Roger, 1997), an approach specifically proposed for small sample settings. Normality of residuals from the mixed models was assessed using the Shapiro-Wilk test, and a Box-Cox transformed (Box and Cox, 1964) outcome variable for dendritic length was used when departure from normality was detected. Sholl analyses of dendritic branch node and intersection frequency were similarly analyzed using a generalized linear mixed model, except assuming the data follow a Poisson instead of a normal distribution. Also, an additional scale parameter was included to increase model flexibility and account for over-dispersion. Owing to the relatively small number of animals sampled, genotypic differences at each radius were considered statistically significant if the raw p-value was less than 0.05. All tests were two-tailed.

Results

Demonstration of Met signaling deficiency in the cortex of $Emx1^{Cre}/Met^{fx/fx}$ mice

A previous study reporting a Cre recombinase-driven deletion of the Met^{fx} allele from hepatocytes demonstrated successful removal of the ATP-binding site from the Met tyrosine kinase domain, and consequently, dramatic reductions in levels of signaling-competent Met

protein, receptor activation and downstream signaling (Huh et al., 2004). We confirmed similar Met signaling deficiencies in forebrain tissues derived from the dorsal pallium in $Emx1^{Cre}/Met^{fx/fx}$ mice during the period of peak receptor expression in the postnatal mouse forebrain (Judson et al., 2009). First, a dramatically reduced ratio of processed (140 kD), presumably signaling-competent Met to unprocessed (170 kD) precursor protein was immunoprecipitated from lysates of $Emx1^{Cre}/Met^{fx/fx}$ postnatal day (P) 7 neocortex relative to wild type (Fig. 1A). Second, we observed a robust induction of Met receptor phosphorylation in HGF-stimulated synaptosomes prepared from P7 wild type but not $Emx1^{Cre}/Met^{fx/fx}$ synaptosomes (Fig. 1B). Collectively, these data demonstrate the utility of the $Emx1^{Cre}/Met^{fx/fx}$ mouse as a model in which to study the consequences of Met signaling deficiency during forebrain circuit development.

Met-dependent changes in layer- and compartment-specific dendritic arbors in pyramidal neurons of anterior cingulate cortex

To begin to understand the effects of attenuated Met signaling on forebrain circuit development, we focused on comparisons of dendritic morphology in wild type and $Emx1^{Cre}/Met^{fx/fx}$ pyramidal neurons of the anterior cingulate cortex (ACC) at a time-point (P40) just subsequent to the most robust periods of circuit connectivity and refinement. ACC pyramidal neurons presented as a compelling population for study for 3 reasons: 1) these neurons act as key integrators and processors of limbic circuit information, 2) these neurons constitute a Met-expressing population shared by mouse and non-human primate cortex (M. Judson, D. Amaral, P. Levitt, unpublished observations) and 3) corticocortical afferents to ACC pyramidal neurons express abundant levels of Met during limbic circuit formation, raising the possibility that dendritic morphologies of these neurons in $Emx1^{Cre}/Met^{fx/fx}$ mice would reflect both cell-autonomous and circuit-level effects of Met signaling disruption. To visualize and study ACC pyramidal dendrites, we employed the Lucifer Yellow microinjection technique, which allowed for the reliable sampling of both layer 5 and layer 2/3 pyramidals (Figs. 2A and 3A) as well as the faithful three-dimensional (3D) reconstruction of dendritic arbors and analysis of several morphometric parameters.

Contrary to the reported growth-promoting effects of HGF-signaling *in vitro*, but consistent with grossly normal ACC cytoarchitecture and histology (Judson et al., 2009), no statistically significant differences were found in the number of primary dendrites (Suppl. Fig. 1A,B), total dendritic arbor length (Figs. 2C, 3C), or total apical or basal dendritic arbor length (**data not shown**) between wild type and $Emx1^{Cre}/Met^{fx/fx}$ ACC pyramidal neurons. Qualitative comparisons of representative neuronal traces (Figs. 2B, 3B), however, suggested altered dendritic length distributions within the arbors of layer 5 and layer 2/3 $Emx1^{Cre}/Met^{fx/fx}$ pyramidal neurons. Moreover, these differences appeared specific to distinct arbor regions and compartments and were resolved quantitatively using Sholl analyses. A reduction in total dendritic length distal to the soma was shared by layer 5 and layer 2/3 $Emx1^{Cre}/Met^{fx/fx}$ pyramidal neurons (Figs. 2D,3D), and was corroborated by decreases in branching complexity in the same arbor regions (Figs. 2E, 3E). Additional, separate Sholl analyses of the apical and basal arbors alone indicated that these changes were specific to the apical dendritic compartment (Figs. 2G, 3G). Finally, as demonstrated by 3D convex hull analysis, which measures the volume contained within the arbor's most outward lying dendritic end-points (Suppl. Fig. 2A–D), the loss in distal apical length translated into an approximate 20% reduction in the average cortical volume sampled by $Emx1^{Cre}/Met^{fx/fx}$ ACC pyramidal neurons (Figs. 2H, 3H). Interestingly, despite these broad phenotypic similarities, there were different causes underlying the apical arbor deficits in these two groups of $Emx1^{Cre}/Met^{fx/fx}$ ACC pyramidal neurons. Specifically, the reduction in apical arbor length in layer 5 mutantpyramidal neurons were primarily a function of reduced average dendritic segment length (Suppl. Fig. 3A,C), whereas those in layer 2/3 pyramidal

neurons were caused by reduced branching in select regions of the apical arbor (Suppl. Fig. 4A,C).

$Emx1^{Cre}/Met^{fx/fx}$ layer 5 and layer 2/3 ACC pyramidal neurons differed with regard to dendritic length proximal to the cell body (Figs. 2D, 3D). As revealed by Sholl analyses of the total dendritic arbor, proximal dendritic length and branching complexity (Fig. 3D,E) was significantly increased in $Emx1^{Cre}/Met^{fx/fx}$ layer 2/3 pyramidal neurons. Further compartment-specific analysis indicated that this difference was specific to the basal arbor (Fig 3F) and likely due to robust increases in branching (Suppl. Fig. 4A). This occurred despite a trend toward modestly reduced average basal dendritic segment length in these cells (Suppl. Fig. 4B). The distribution of dendritic length both proximal to the cell body and within the basal arbors of $Emx1^{Cre}/Met^{fx/fx}$ layer 5 pyramidal neurons was statistically indistinguishable from that in wild type neurons (Fig. 2D,F). There was, however, a trend toward reduced basal dendritic segment length in these cells (Suppl. Fig. 3B). These data suggest that in the absence of Met signaling, there are different adaptive changes in distinct neuronal compartments that may reflect circuit-specific influences.

Met-dependent changes in spine head size on ACC pyramidal neurons

Changes in the dendritic morphology of $Emx1^{Cre}/Met^{fx/fx}$ ACC pyramidal neurons were layer-specific in nature, prompting us to determine whether or not dendritic spine morphology across layers might also be differentially susceptible to Met signaling deficiency. Therefore, we focused on dendritic spines in the basal compartment of layer 5 and layer 2/3 neurons where layer-specific differences in dendritic branching were most clear.

Using high resolution 3D renderings of confocal image stacks, we analyzed 5,064 spines in layer 5 basal dendritic segments and 7,197 spines in layer 2/3 basal dendritic segments for the purpose of assessing potential genotypic differences in spine density and spine head volume. Neither layer 5 (Fig. 4M) nor layer 2/3 (Fig. 5M) neurons exhibited changes in basal dendritic spine density in the $Emx1^{Cre}/Met^{fx/fx}$ as compared to wild type ACC. However, statistically significant increases in spine head volume were detected in both populations of $Emx1^{Cre}/Met^{fx/fx}$ cells (Figs. 4N, 5N). The data also revealed a rightward shift in the frequency distribution of $Emx1^{Cre}/Met^{fx/fx}$ versus wild type basal dendritic spine head volumes. An approximate 20–25% reduction in the presence of the thinnest spine classes was the most statistically robust finding (Figs. 4O,5O). Collectively, these data demonstrate similar alterations in dendritic spine morphology on arbors whose branching morphologies are differentially affected by disrupted Met signaling.

Met-dependent changes in dendritic arbors and spine morphology in striatal medium spiny neurons

We analyzed the dendritic morphology of Lucifer Yellow-injected dorsolateral MSNs from the same wild type and $Emx1^{Cre}/Met^{fx/fx}$ mice used to study the morphology of ACC pyramidal neurons. Measures of total dendritic length revealed an approximate 20% increase in the dendritic arbors of MSNs in $Emx1^{Cre}/Met^{fx/fx}$ mice compared to wild type (Fig. 6C). This difference in dendritic growth is robust and readily appreciated qualitatively in two-dimensional projections of Neurolucida tracings (Fig. 6B). Sholl analysis of the distribution of dendritic length (Fig. 6D) revealed increases in the $Emx1^{Cre}/Met^{fx/fx}$ arbors beginning approximately 50 μM from the cell body and spanning the extent of the arbor. This finding is consistent with there being equivalent numbers of primary dendrites (Suppl. Fig. 1C), but increased branching (Fig. 6F) and branching complexity (Fig 6E) of higher order dendrites, in the $Emx1^{Cre}/Met^{fx/fx}$ arbors relative to wild type. Furthermore, we found that the

approximate 20% increase in $Emx1^{Cre}/Met^{fx/fx}$ MSN dendritic arbor volume (Fig. 6H) was not due to an increase in the average length of dendritic segments (Fig. 6G).

At the level of the dendritic spine, we also detected significant morphological differences in the $Emx1^{Cre}/Met^{fx/fx}$ MSN arbors. We analyzed a total of 7,573 MSN spines across genotypic groups. Relative to wild type MSN dendrites, dendritic spine density was normal (Fig. 7M), but average spine head volume was increased by approximately 12% (Fig. 7N), and the frequency distribution of spine head size revealed a reduced proportion of the smallest spines (Fig. 7O). Consequently, the overall dendritic phenotype of $Emx1^{Cre}/Met^{fx/fx}$ MSNs, which do not express Met, is reminiscent of the basal dendrites of layer 2/3 ACC pyramidal neurons. The collective data from neocortex and striatum suggest that disruption of Met signaling influences developing forebrain neurons in a circuit-dependent fashion.

Discussion

The major finding of this study is that the constitutive elimination of Met receptor tyrosine kinase signaling during development *in vivo* results in cell-nonautonomous changes in dendrite and dendritic spine morphology in forebrain neurons (Suppl. Tables 1 and 2). Two critical features of our experimental approach allowed us to dissociate these changes from cell-autonomous effects on dendritic structure- a considerable challenge considering the well-documented roles for Met signaling in dendritic (Gutierrez et al., 2004; Tyndall et al., 2007; Lim and Walikonis, 2008) and axonal outgrowth *in vitro* (Ebens et al., 1996; David et al., 2008) as well as the localization of Met to both dendritic and axonal compartments *in vivo* (Tyndall and Walikonis, 2006; Judson et al., 2009). First, based on transcript and protein expression, Met expression is absent or expressed at very low levels in medium spiny neurons (MSN) in the developing pre- and postnatal striatum (Judson et al., 2009), suggesting that any alterations in their dendritic morphology subsequent to an ablation of Met signaling is not cell-autonomous in nature. Second, in the $Emx1^{Cre}/Met^{fx/fx}$ mouse, Met signaling is ablated from nearly all Met-expressing MSN afferents during development (Judson et al., 2009), rendering these cells vulnerable to cell-nonautonomous, presynaptically-derived changes in dendritic morphology. We documented such changes in $Emx1^{Cre}/Met^{fx/fx}$ MSN dendritic morphology using the Lucifer Yellow microinjection technique. Specifically, we detected a marked increase in dendritic branching and total dendritic length and a significant increase in dendritic spine head volume in $Emx1^{Cre}/Met^{fx/fx}$ MSN neurons relative to their wild type counterparts (Suppl. Table 1). Because similar changes in dendritic morphology were detected in the basal arbors of $Emx1^{Cre}/Met^{fx/fx}$ ACC pyramidal neurons (Suppl. Tables 1 and 2), it is possible that these circuit-level influences affect all dendritic compartments that receive Met-expressing axonal afferents.

Mechanisms of altered dendrite and dendritic spine morphology in the $Emx1^{Cre}/Met^{fx/fx}$ forebrain

This study provides, to our knowledge, the first evidence that Met signaling can influence the development of dendrites on select forebrain neurons in a circuit-related fashion. However, the mechanistic nature of the influences is unclear. One possibility is that Met signals directly within the developing pre-terminal axon to impact postsynaptic neuronal development. Though this signaling capacity has yet to be directly demonstrated, its potential is supported by observations of upregulated Met expression in the terminal fields of forebrain axons during, but not prior to, robust periods of axon collateralization and the beginning of synaptogenesis (Judson et al., 2009). Assuming that Met signals within presynaptic compartments, elucidating its role in regulating presynaptic function will require additional morphological and electrophysiological analyses.

There are examples in the literature that would be consistent with the resultant MSN adaptive changes due to either increased or reduced presynaptic signaling. For example, both broad (Dierssen et al., 2003; Gelfo et al., 2009) and focal (Russell and Moore, 1999; Sorensen and Rubel, 2006) manipulations of afferent activity have been shown to positively correlate with changes in dendritic structure, suggesting that the enhanced branching in $Emx1^{Cre}/Met^{fx/fx}$ MSN dendritic arbors could result from increased corticostriatal afferent activity. This would imply that Met signaling normally serves to limit corticostriatal activity and neurotransmitter release. Alternatively, reduced afferent activity or a mistargeting of presynaptic elements can sometimes evoke paradoxical increases in dendritic growth (Lund et al., 1991; McAllister et al., 1996; Tripodi et al., 2008). Such a scenario would require Met signaling to potentiate corticostriatal activity, perhaps during earlier developmental periods when pre- and postsynaptic elements are establishing initial contact (McAllister, 2000). Presynaptic roles for Met signaling are similarly difficult to predict from changes in $Emx1^{Cre}/Met^{fx/fx}$ MSN dendritic spine morphology. Larger spine heads predict stronger synapses (Schikorski and Stevens, 1997; Murthy et al., 2001), which could have been sculpted by increases in corticostriatal afferent activity and trophic support in $Emx1^{Cre}/Met^{fx/fx}$ mice. Alternatively, increased spine size may reflect a homeostatic scaling up of $Emx1^{Cre}/Met^{fx/fx}$ MSN excitability in response to decreased excitatory drive from corticostriatal afferents. Complimentary morphometric and electrophysiological studies of corticostriatal connectivity in the $Emx1^{Cre}/Met^{fx/fx}$ mouse are ongoing, and will clarify Met signaling roles in axonal and presynaptic development. The distinct laminar- and compartment-specific changes expressed by ACC pyramidal neurons following disruption of Met signaling (Suppl. Table 3) also suggest circuit-level influences on dendritic growth. However, because cortical afferents, efferents and intrinsic neurons express Met, distinguishing between cell-autonomous and presynaptically-driven effects of Met signaling will be challenging.

Implications of $Emx1^{Cre}/Met^{fx/fx}$ dendrite and dendritic spine phenotypes for cellular and circuit function

The dendritic phenotypes of the $Emx1^{Cre}/Met^{fx/fx}$ neurons offer insight regarding the effects of Met signaling disruptions at the single cell- and circuit-levels. Moderate to large increases in average spine head volume were found consistently across anatomical regions. As head volume is the spine morphometric parameter most positively correlated with postsynaptic density size (Arellano et al., 2007), it is reasonable to assume that excitatory synapses are significantly larger in $Emx1^{Cre}/Met^{fx/fx}$ neurons. Moreover, hippocampal slice studies indicate that increases in spine head volume of the magnitude detected here (i.e., 12–25%) result in large increases in the amplitude of excitatory postsynaptic currents (Matsuzaki et al., 2001).

Frequency distributions of dendritic spine head volume specifically indicate a gain of larger spines at the expense of thinner, presumably more labile varieties. This is consistent with a possible impact on neuronal plasticity. Increases in dendritic spine size accompany the induction of long-term potentiation (LTP) (Engert and Bonhoeffer, 1999; Park et al., 2006; Roberts et al., 2009). In $Emx1^{Cre}/Met^{fx/fx}$ neurons, in which spine size is already shifted toward maximal levels, there may be a reduced potential to induce, or further increase, LTP. In fact, this is consistent with preliminary findings in hippocampal slices from $Emx1^{Cre}/Met^{fx/fx}$ mice in which the induction and sustainability of LTP is reduced (S. Qiu and P. Levitt, unpublished observations).

Developmentally, Met expression begins to decline during the second postnatal week (Judson et al., 2009), coinciding with changes in presynaptic release probability (Bolshakov and Siegelbaum, 1995; Chavis and Westbrook, 2001) and postsynaptic excitability (Sheng et al., 1994; Petralia et al., 1999; Elias et al., 2008). This raises the possibility that Met signals

to maintain developing synapses in an immature, labile state and that the ablation of Met signaling in $Emx1^{Cre}/Met^{fx/fx}$ mice might result in a precocious maturation of synaptic connections- a postulate tentatively supported by our observation of increased spine head volume in the dendrites of P40 $Emx1^{Cre}/Met^{fx/fx}$ neurons. An early onset of robust LTP induction (Harris and Teyler, 1984; Muller et al., 1989), premature gains in postsynaptic density size and thickness (Welch et al., 2007; Hung et al., 2008; Roberts et al., 2009), and shifts in NMDAR subunit composition (Sheng et al., 1994; Flint et al., 1997; Roberts et al., 2009) constitute logical phenotypic predictions for these mice if they indeed mature precociously. Of course, considering the potential for Met to signal in both postsynaptic and presynaptic compartments, these hypotheses will be addressed best by electrophysiological and biochemical studies of corticocortical as well as corticostriatal synapses.

The approximate 20% reduction in $Emx1^{Cre}/Met^{fx/fx}$ ACC pyramidal dendritic arbor volume indicates potentially significant alterations in information processing at the circuit-level. This reduction was due to decreases in dendritic length at approximately 150–175 μM in radial distance from the cell body, changes that were restricted to the apical arbor. Importantly, in layer 5 $Emx1^{Cre}/Met^{fx/fx}$ ACC pyramidal neurons, this phenotype is explained entirely by shorter oblique apical branches, because the apical dendrite of these neurons was always transected before the bifurcation node and apical tuft. This change could be functionally significant for several reasons. For example, topographical mapping of inputs to layer 5 neurons in somatosensory cortex suggests that oblique branches of the apical arbor are an important convergence point of ascending thalamic and descending cortical information (Petreanu et al., 2009). In addition, in general terms, a loss of distal relative to proximal dendritic length should restrict the cortical territory sampled by a pyramidal neuron, which could limit the integration of information across the tangential domain. This functional consequence would be most relevant to the apical dendritic tuft, which receives highly convergent inputs from both the cortex (Kuhn et al., 2008; Petreanu et al., 2009) and the thalamus (Jones, 2002; Rubio-Garrido et al., 2009) that facilitate attention and associative processing. This dendritic domain remains to be studied in the $Emx1^{Cre}/Met^{fx/fx}$ mouse.

Contrary to ACC pyramidal neurons, striatal MSNs exhibited an approximate 25% increase in dendrite arbor volume in $Emx1^{Cre}/Met^{fx/fx}$ mice, implying that they are capable of receiving more broadly distributed striatal afferents. Considering the patch-matrix compartmental organization of the striatum, this change could affect the quality of discrete information processing. MSN dendritic arbors are largely confined to the compartment of their cell body of origin (Gerfen, 1992), so without concomitant decreases in striatal cell density, the larger arbors of $Emx1^{Cre}/Met^{fx/fx}$ MSNs would be expected to extend beyond their compartmental boundaries. This might result in an atypical mixing of afferent sensorimotor and limbic information that usually is routed through the matrix and patch compartments, respectively (Gerfen, 1992).

Relevance of Met signaling disruptions to circuit vulnerability in ASD

Our observation of altered dendritic morphology in MSNs in $Emx1^{Cre}/Met^{fx/fx}$ mice demonstrates the potential for presynaptic Met signaling to regulate the development of long-range forebrain circuits. This finding may have relevance to findings of global forebrain hypoconnectivity in ASD (Just et al., 2004; Koshino et al., 2008; Perez Velazquez et al., 2009). Local hyperconnectivity has also been proposed in ASD (Casanova et al., 2002; Casanova, 2006), and the layer- and especially compartment-specific nature of the dendritic phenotypes in the $Emx1^{Cre}/Met^{fx/fx}$ ACC may reflect local circuit disruptions. However, electrophysiological studies such as those performed by Markram and colleagues (Rinaldi et al., 2008a; Rinaldi et al., 2008b) in the valproic acid rat model of autism will be

required before definitive conclusions about local cortical connectivity in the $Emx1^{Cre/}$ $Met^{fx/fx}$ mouse can be made.

We further suggest that even mild disruptions in Met signaling may render select circuits that express the receptor vulnerable to further genetic and environmental insults that would otherwise more broadly impact connectivity (Campbell et al., 2008; Bill and Geschwind, 2009; Judson et al., 2009). Analyses of $Emx1^{Cre}/Met^{fx/+}$ mice in compound genetic and/or environmental models of forebrain circuit disruption will constitute a useful test of this hypothesis. Additionally, mapping the expression of MET during the development of the human and nonhuman primate forebrain may promote a further understanding of the specific circuits that are vulnerable in ASD.

Supplementary Material

Refer to Web version on PubMed Central for supplementary material.

Acknowledgments

Grant sponsor: National Institutes of Health (NIH)/National Institute of Mental Health (NIMH); Grant number MH067842 (PL); Grant Sponsor: NIH/National Institute of Child Health and Human Development; Grant number: P30 HD15052 (E. Dykens); Grant sponsor: NIH/National Institute on Drug Abuse (NIDA); Grant number DA022785 (PL); Simons Foundation (PL)

We thank Deborah Gregory, Donte Smith, and Kate Spencer for excellent assistance in maintaining the mouse colony and genotyping. We also thank Drs. Inmaculada Ballesteros-Yanez and Ariel Deutch for the generous introduction to the Lucifer Yellow injection technique and use of the Imaris software, respectively.

Literature Cited

Arellano JI, Benavides-Piccione R, Defelipe J, Yuste R. Ultrastructure of dendritic spines: correlation between synaptic and spine morphologies. Front Neurosci. 2007; 1(1):131–143. [PubMed: 18982124]

Bill BR, Geschwind DH. Genetic advances in autism: heterogeneity and convergence on shared pathways. Curr Opin Genet Dev. 2009; 19(3):271–278. [PubMed: 19477629]

Bolshakov VY, Siegelbaum SA. Regulation of hippocampal transmitter release during development and long-term potentiation. Science. 1995; 269(5231):1730–1734. [PubMed: 7569903]

Campbell DB, D'Oronzio R, Garbett K, Ebert PJ, Mirnics K, Levitt P, Persico AM. Disruption of cerebral cortex MET signaling in autism spectrum disorder. Ann Neurol. 2007; 62(3):243–250. [PubMed: 17696172]

Campbell DB, Li C, Sutcliffe JS, Persico AM, Levitt P. Genetic evidence implicating multiple genes in the MET receptor tyrosine kinase pathway in autism spectrum disorder. Autism Research. 2008; 1:159–168. [PubMed: 19360663]

Campbell DB, Sutcliffe JS, Ebert PJ, Militerni R, Bravaccio C, Trillo S, Elia M, Schneider C, Melmed R, Sacco R, Persico AM, Levitt P. A genetic variant that disrupts MET transcription is associated with autism. Proc Natl Acad Sci U S A. 2006; 103(45):16834–16839. [PubMed: 17053076]

Campbell DB, Warren D, Sutcliffe JS, Lee EB, Levitt P. Association of MET with social and communication phenotypes in individuals with autism spectrum disorder. Am J Med Genet B Neuropsychiatr Genet. 2009

Casanova MF. Neuropathological and genetic findings in autism: the significance of a putative minicolumnopathy. Neuroscientist. 2006; 12(5):435–441. [PubMed: 16957005]

Casanova MF, Buxhoeveden DP, Switala AE, Roy E. Minicolumnar pathology in autism. Neurology. 2002; 58(3):428–432. [PubMed: 11839843]

Caton A, Hacker A, Naeem A, Livet J, Maina F, Bladt F, Klein R, Birchmeier C, Guthrie S. The branchial arches and HGF are growth-promoting and chemoattractant for cranial motor axons. Development (Cambridge, England). 2000; 127(8):1751–1766.

Chavis P, Westbrook G. Integrins mediate functional pre- and postsynaptic maturation at a hippocampal synapse. Nature. 2001; 411(6835):317–321. [PubMed: 11357135]

David MD, Yeramian A, Dunach M, Llovera M, Canti C, de Herreros AG, Comella JX, Herreros J. Signalling by neurotrophins and hepatocyte growth factor regulates axon morphogenesis by differential beta-catenin phosphorylation. J Cell Sci. 2008; 121(Pt 16):2718–2730. [PubMed: 18664491]

Dierssen M, Benavides-Piccione R, Martinez-Cue C, Estivill X, Florez J, Elston GN, DeFelipe J. Alterations of neocortical pyramidal cell phenotype in the Ts65Dn mouse model of Down syndrome: effects of environmental enrichment. Cereb Cortex. 2003; 13(7):758–764. [PubMed: 12816891]

Ebens A, Brose K, Leonardo ED, Hanson MG Jr, Bladt F, Birchmeier C, Barres BA, Tessier-Lavigne M. Hepatocyte growth factor/scatter factor is an axonal chemoattractant and a neurotrophic factor for spinal motor neurons. Neuron. 1996; 17(6):1157–1172. [PubMed: 8982163]

Elias GM, Elias LA, Apostolides PF, Kriegstein AR, Nicoll RA. Differential trafficking of AMPA and NMDA receptors by SAP102 and PSD-95 underlies synapse development. Proc Natl Acad Sci U S A. 2008; 105(52):20953–20958. [PubMed: 19104036]

Engert F, Bonhoeffer T. Dendritic spine changes associated with hippocampal long-term synaptic plasticity. Nature. 1999; 399(6731):66–70. [PubMed: 10331391]

Flint AC, Maisch US, Weishaupt JH, Kriegstein AR, Monyer H. NR2A subunit expression shortens NMDA receptor synaptic currents in developing neocortex. J Neurosci. 1997; 17(7):2469–2476. [PubMed: 9065507]

Garzotto D, Giacobini P, Crepaldi T, Fasolo A, De Marchis S. Hepatocyte growth factor regulates migration of olfactory interneuron precursors in the rostral migratory stream through Met-Grb2 coupling. J Neurosci. 2008; 28(23):5901–5909. [PubMed: 18524894]

Gelfo F, De Bartolo P, Giovine A, Petrosini L, Leggio MG. Layer and regional effects of environmental enrichment on the pyramidal neuron morphology of the rat. Neurobiol Learn Mem. 2009; 91(4):353–365. [PubMed: 19340947]

Gerfen CR. The neostriatal mosaic: multiple levels of compartmental organization. Trends Neurosci. 1992; 15(4):133–139. [PubMed: 1374971]

Giacobini P, Messina A, Wray S, Giampietro C, Crepaldi T, Carmeliet P, Fasolo A. Hepatocyte growth factor acts as a motogen and guidance signal for gonadotropin hormone-releasing hormone-1 neuronal migration. J Neurosci. 2007; 27(2):431–445. [PubMed: 17215404]

Gorski JA, Talley T, Qiu M, Puelles L, Rubenstein JL, Jones KR. Cortical excitatory neurons and glia, but not GABAergic neurons, are produced in the Emx1-expressing lineage. J Neurosci. 2002; 22(15):6309–6314. [PubMed: 12151506]

Gutierrez H, Dolcet X, Tolcos M, Davies A. HGF regulates the development of cortical pyramidal dendrites. Development (Cambridge, England). 2004; 131(15):3717–3726.

Hamanoue M, Takemoto N, Matsumoto K, Nakamura T, Nakajima K, Kohsaka S. Neurotrophic effect of hepatocyte growth factor on central nervous system neurons in vitro. Journal of neuroscience research. 1996; 43(5):554–564. [PubMed: 8833090]

Harris KM, Teyler TJ. Developmental onset of long-term potentiation in area CA1 of the rat hippocampus. J Physiol. 1984; 346:27–48. [PubMed: 6699775]

Huh CG, Factor VM, Sanchez A, Uchida K, Conner EA, Thorgeirsson SS. Hepatocyte growth factor/c-met signaling pathway is required for efficient liver regeneration and repair. Proc Natl Acad Sci U S A. 2004; 101(13):4477–4482. [PubMed: 15070743]

Hung AY, Futai K, Sala C, Valtschanoff JG, Ryu J, Woodworth MA, Kidd FL, Sung CC, Miyakawa T, Bear MF, Weinberg RJ, Sheng M. Smaller dendritic spines, weaker synaptic transmission, but enhanced spatial learning in mice lacking Shank1. J Neurosci. 2008; 28(7):1697–1708. [PubMed: 18272690]

Ieraci A, Forni PE, Ponzetto C. Viable hypomorphic signaling mutant of the Met receptor reveals a role for hepatocyte growth factor in postnatal cerebellar development. Proc Natl Acad Sci U S A. 2002; 99(23):15200–15205. [PubMed: 12397180]

Jackson PB, Boccuto L, Skinner C, Collins JS, Neri G, Gurrieri F, Schwartz CE. Further evidence that the rs1858830 C variant in the promoter region of the MET gene is associated with autistic disorder. Autism Res. 2009; 2(4):232–236. [PubMed: 19681062]

Jones EG. Thalamic circuitry and thalamocortical synchrony. Philos Trans R Soc Lond B Biol Sci. 2002; 357(1428):1659–1673. [PubMed: 12626002]

Judson MC, Bergman MY, Campbell DB, Eagleson KL, Levitt P. Dynamic gene and protein expression patterns of the autism-associated met receptor tyrosine kinase in the developing mouse forebrain. J Comp Neurol. 2009; 513(5):511–531. [PubMed: 19226509]

Just MA, Cherkassky VL, Keller TA, Minshew NJ. Cortical activation and synchronization during sentence comprehension in high-functioning autism: evidence of underconnectivity. Brain. 2004; 127(Pt 8):1811–1821. [PubMed: 15215213]

Kenward MG, Roger JH. Small sample inference for fixed effects from restricted maximum likelihood. Biometrics. 1997; 53(3):983–997. [PubMed: 9333350]

Koshino H, Kana RK, Keller TA, Cherkassky VL, Minshew NJ, Just MA. fMRI investigation of working memory for faces in autism: visual coding and underconnectivity with frontal areas. Cereb Cortex. 2008; 18(2):289–300. [PubMed: 17517680]

Kuhn B, Denk W, Bruno RM. In vivo two-photon voltage-sensitive dye imaging reveals top-down control of cortical layers 1 and 2 during wakefulness. Proc Natl Acad Sci U S A. 2008; 105(21): 7588–7593. [PubMed: 18508976]

Lim CS, Walikonis RS. Hepatocyte growth factor and c-Met promote dendritic maturation during hippocampal neuron differentiation via the Akt pathway. Cell Signal. 2008; 20(5):825–835. [PubMed: 18262389]

Lund JS, Holbach SM, Chung WW. Postnatal development of thalamic recipient neurons in the monkey striate cortex: II. Influence of afferent driving on spine acquisition and dendritic growth of layer 4C spiny stellate neurons. J Comp Neurol. 1991; 309(1):129–140. [PubMed: 1894766]

Madhavan R, Peng HB. HGF induction of postsynaptic specializations at the neuromuscular junction. J Neurobiol. 2006; 66(2):134–147. [PubMed: 16215993]

Matsuzaki M, Ellis-Davies GC, Nemoto T, Miyashita Y, Iino M, Kasai H. Dendritic spine geometry is critical for AMPA receptor expression in hippocampal CA1 pyramidal neurons. Nat Neurosci. 2001; 4(11):1086–1092. [PubMed: 11687814]

McAllister AK. Cellular and molecular mechanisms of dendrite growth. Cereb Cortex. 2000; 10(10): 963–973. [PubMed: 11007547]

McAllister AK, Katz LC, Lo DC. Neurotrophin regulation of cortical dendritic growth requires activity. Neuron. 1996; 17(6):1057–1064. [PubMed: 8982155]

Muller D, Oliver M, Lynch G. Developmental changes in synaptic properties in hippocampus of neonatal rats. Brain Res Dev Brain Res. 1989; 49(1):105–114.

Murthy VN, Schikorski T, Stevens CF, Zhu Y. Inactivity produces increases in neurotransmitter release and synapse size. Neuron. 2001; 32(4):673–682. [PubMed: 11719207]

Nakano M, Takagi N, Takagi K, Funakoshi H, Matsumoto K, Nakamura T, Takeo S. Hepatocyte growth factor promotes the number of PSD-95 clusters in young hippocampal neurons. Exp Neurol. 2007; 207(2):195–202. [PubMed: 17678646]

Park M, Salgado JM, Ostroff L, Helton TD, Robinson CG, Harris KM, Ehlers MD. Plasticity-induced growth of dendritic spines by exocytic trafficking from recycling endosomes. Neuron. 2006; 52(5): 817–830. [PubMed: 17145503]

Perez Velazquez JL, Barcelo F, Hung Y, Leshchenko Y, Nenadovic V, Belkas J, Raghavan V, Brian J, Garcia Dominguez L. Decreased brain coordinated activity in autism spectrum disorders during executive tasks: reduced long-range synchronization in the fronto-parietal networks. Int J Psychophysiol. 2009; 73(3):341–349. [PubMed: 19465065]

Petralia RS, Esteban JA, Wang YX, Partridge JG, Zhao HM, Wenthold RJ, Malinow R. Selective acquisition of AMPA receptors over postnatal development suggests a molecular basis for silent synapses. Nat Neurosci. 1999; 2(1):31–36. [PubMed: 10195177]

Petreanu L, Mao T, Sternson SM, Svoboda K. The subcellular organization of neocortical excitatory connections. Nature. 2009; 457(7233):1142–1145. [PubMed: 19151697]

Powell EM, Muhlfriedel S, Bolz J, Levitt P. Differential regulation of thalamic and cortical axonal growth by hepatocyte growth factor/scatter factor. Dev Neurosci. 2003; 25(2–4):197–206. [PubMed: 12966217]

Rinaldi T, Perrodin C, Markram H. Hyper-connectivity and hyper-plasticity in the medial prefrontal cortex in the valproic Acid animal model of autism. Front Neural Circuits. 2008a; 2:4. [PubMed: 18989389]

Rinaldi T, Silberberg G, Markram H. Hyperconnectivity of local neocortical microcircuitry induced by prenatal exposure to valproic acid. Cereb Cortex. 2008b; 18(4):763–770. [PubMed: 17638926]

Roberts AC, Diez-Garcia J, Rodriguiz RM, Lopez IP, Lujan R, Martinez-Turrillas R, Pico E, Henson MA, Bernardo DR, Jarrett TM, Clendeninn DJ, Lopez-Mascaraque L, Feng G, Lo DC, Wesseling JF, Wetsel WC, Philpot BD, Perez-Otano I. Downregulation of NR3A-containing NMDARs is required for synapse maturation and memory consolidation. Neuron. 2009; 63(3):342–356. [PubMed: 19679074]

Rosario M, Birchmeier W. How to make tubes: signaling by the Met receptor tyrosine kinase. Trends Cell Biol. 2003; 13(6):328–335. [PubMed: 12791299]

Rubio-Garrido P, Perez-de-Manzo F, Porrero C, Galazo MJ, Clasca F. Thalamic input to distal apical dendrites in neocortical layer 1 is massive and highly convergent. Cereb Cortex. 2009; 19(10): 2380–2395. [PubMed: 19188274]

Russell FA, Moore DR. Effects of unilateral cochlear removal on dendrites in the gerbil medial superior olivary nucleus. Eur J Neurosci. 1999; 11(4):1379–1390. [PubMed: 10103133]

Schikorski T, Stevens CF. Quantitative ultrastructural analysis of hippocampal excitatory synapses. J Neurosci. 1997; 17(15):5858–5867. [PubMed: 9221783]

Shen H, Sesack SR, Toda S, Kalivas PW. Automated quantification of dendritic spine density and spine head diameter in medium spiny neurons of the nucleus accumbens. Brain Struct Funct. 2008; 213(1–2):149–157. [PubMed: 18535839]

Sheng M, Cummings J, Roldan LA, Jan YN, Jan LY. Changing subunit composition of heteromeric NMDA receptors during development of rat cortex. Nature. 1994; 368(6467):144–147. [PubMed: 8139656]

Sholl DA. Dendritic organization in the neurons of the visual and motor cortices of the cat. J Anat. 1953; 87(4):387–406. [PubMed: 13117757]

Sorensen SA, Rubel EW. The level and integrity of synaptic input regulates dendrite structure. J Neurosci. 2006; 26(5):1539–1550. [PubMed: 16452677]

Sousa I, Clark TG, Toma C, Kobayashi K, Choma M, Holt R, Sykes NH, Lamb JA, Bailey AJ, Battaglia A, Maestrini E, Monaco AP. MET and autism susceptibility: family and case-control studies. Eur J Hum Genet. 2009; 17(6):749–758. [PubMed: 19002214]

Tripodi M, Evers JF, Mauss A, Bate M, Landgraf M. Structural homeostasis: compensatory adjustments of dendritic arbor geometry in response to variations of synaptic input. PLoS Biol. 2008; 6(10):e260. [PubMed: 18959482]

Tyndall SJ, Patel SJ, Walikonis RS. Hepatocyte growth factor-induced enhancement of dendritic branching is blocked by inhibitors of N-methyl-D-aspartate receptors and calcium/calmodulin-dependent kinases. Journal of neuroscience research. 2007; 85(11):2343–2351. [PubMed: 17600375]

Tyndall SJ, Walikonis RS. The receptor tyrosine kinase Met and its ligand hepatocyte growth factor are clustered at excitatory synapses and can enhance clustering of synaptic proteins. Cell Cycle. 2006; 5(14):1560–1568. [PubMed: 16861928]

Welch JM, Lu J, Rodriguiz RM, Trotta NC, Peca J, Ding JD, Feliciano C, Chen M, Adams JP, Luo J, Dudek SM, Weinberg RJ, Calakos N, Wetsel WC, Feng G. Cortico-striatal synaptic defects and OCD-like behaviours in Sapap3-mutant mice. Nature. 2007; 448(7156):894–900. [PubMed: 17713528]

Zhang YW, Vande Woude GF. HGF/SF-met signaling in the control of branching morphogenesis and invasion. J Cell Biochem. 2003; 88(2):408–417. [PubMed: 12520544]

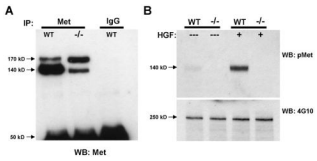

Figure 1.

Met signaling deficiency in the Emx1^{cre}/Met$^{fx/fx}$ mouse. **A:** Total Met Western blotting of Met and control mouse IgG immunoprecipitates from P7 wild type (WT) and Emx1^{cre}/Met$^{fx/fx}$ (−/−) cortical lysates. Note the drastically reduced ratio of processed, signaling-competent Met receptor (140 kD band) to unprocessed receptor precursor (170 kD band) that is immunoprecipitated from the −/− lysate. No Met protein of either form was immunprecipitated with control mouse pre-immune IgG. **B:** Stimulation of P7 crude cortical synaptosomes with 50 ng/ml HGF. Western blotting for phosphorylated Met (pMet) demonstrates that HGF induces substantial Met receptor activation in WT but not −/− synaptosomes. Western blotting for total tyrosine phosphorylated protein (4G10) demonstrates equivalent protein loading across samples.

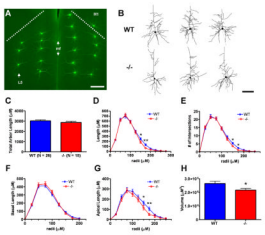

Figure 2.

Analysis of layer 5 pyramidal cell morphometry in postnatal day 40 wild type (WT) versus $Emx1^{cre}/Met^{fx/fx}$ (−/−) anterior cingulate cortex (ACC). **A:** Representative fluorescence micrograph of lucifer yellow immunoreactivity in microinjected pyramidal cells in both left and right anterior cingulate cortex in a coronal brain section. Pyramidal cell injections could be precisely targeted within Layer 5 (arrow, left hemisphere). The dashed lines represent the anatomical boundary between ACC and primary motor cortex (M1) in each hemisphere. The median fissure (mf, double arrows) marks the boundary between hemispheres. Note the absence of immunostaining in uninjected neighboring neurons throughout the tissue. **B:** Representative Neurolucida traces of layer 5 WT and −/− ACC pyramidal neurons. The neurons depicted have dendritic arbor morphometries approximate to the mean values of their genotypic group. **C–H:** Dendritic morphometry summary statistics. Though the average total dendritic arbor lengths are statistically equivalent (C), −/− arbors exhibit reduced dendritic length distal to the cell body (D). Sholl analysis indicates a corroborating reduction in −/− branching complexity in the same distal arbor regions (E). Subcomponent analyses for arbor length indicate that reductions in distal length in −/− layer 5 neurons are due to changes in the apical (G) but not the basal (F) arbor. Three-dimensional convex hull analysis shows that reduced apical arbor length translates into reduced arbor volume in −/− layer 5 pyramidal neurons (H). Scale bar = 275 μM for A and 100 μM for B. **p ≤ 0.01, *p ≤ 0.05.

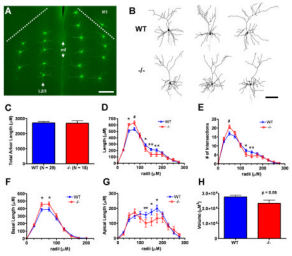

Figure 3.

Analysis of layer 2/3 pyramidal cell morphometry in postnatal day 40 wild type (WT) versus $Emx1^{cre}/Met^{fx/fx}$ (−/−) anterior cingulate cortex (ACC). **A:** Representative fluorescence micrograph of lucifer yellow immunoreactivity in microinjected pyramidal cells in both left and right anterior cingulate cortex in a coronal brain section. Injections of Layer 2/3 pyramidal cells (arrow, left hemisphere) were highly reproducible across animals in terms of radial distance from the pial surface/median fissure (mf). The dashed lines represent the anatomical boundary between ACC and primary motor cortex (M1) in each hemisphere. **B:** Representative Neurolucida traces of layer 2/3 WT and −/− ACC pyramidal neurons. The neurons depicted have dendritic arbor morphometries approximate to the mean values of their genotypic group. **C–H:** Dendritic morphometry summary statistics. Though the average total dendritic arbor lengths are statistically equivalent (C), −/− arbors exhibit *increased* dendritic length proximal to, but *decreased* dendritic length distal to, the cell body (D). Sholl analysis shows that changes in branching complexity in −/− arbors mirror changes in dendritic length as a function of distance from the cell body (E). Subcomponent analyses for arbor length indicate that proximal increases in −/− arbor length reflect changes in the basal arbor (F), while the apical arbor (G) accounts for decreases in distal arbor length. Three-dimensional convex hull analysis reveals a strong trend toward reduced arbor volume in −/− layer 2/3 pyramidal neurons (H), consistent with reduced apical arbor length distal to the cell body. Scale bar = 275 μM for A and 100 μM for B. $^{**}p \leq 0.01$, $^{*}p \leq 0.05$, $^{\#}p \leq 0.1$.

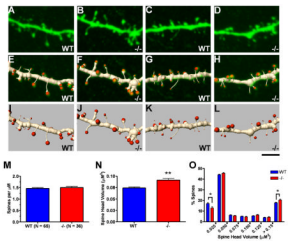

Figure 4.

Analysis of basal dendritic spines in postnatal day 40 wild type (WT) versus Emx1^{cre}/Met$^{fx/fx}$ (−/−) layer 5 pyramidal cells. Confocal projection images of 2 WT (**A** and **C**) and 2 −/− (**B** and **D**) layer 5 pyramidal basal dendritic segments (top row) and associated three-dimensional (3D) segmented renderings shown in overlay (middle row, **E,G** and **F,H**) and apart (bottom row, **I,K** and **J,L**). The images depict portions of analyzed full-length segments with spine density and spine head volume values similar to the mean values of their genotypic group. **M–O:** Quantification of spine density and spine head volume based on 3D renderings. No difference in spine density was observed between genotypic groups (M), but an ~20% increase in average spine head volume was found for −/− layer 5 basal dendritic segments as compared with WT (N). The frequency distribution of spine head volumes reveals greater numbers of larger spines and fewer thinner spines in −/− layer 5 basal dendritic segments (O). Scale bar = 4 μM for all images. **p ≤ 0.01, *p ≤ 0.05.

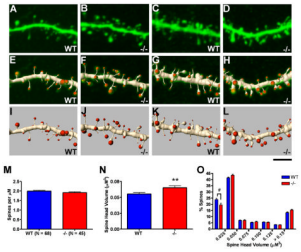

Figure 5.

Analysis of basal dendritic spines in postnatal day 40 wild type (WT) versus Emx1^{cre}/Met$^{fx/fx}$ (−/−) layer 2/3 pyramidal cells. Confocal projection images of 2 WT (**A** and **C**) and 2 −/− (**B** and **D**) layer 2/3 pyramidal basal dendritic segments (top row) and associated three-dimensional (3D) segmented renderings shown in overlay (middle row, **E,G** and **F,H**) and apart (bottom row, **I,K** and **J,L**). The images depict portions of analyzed full-length segments with spine density and spine head volume values similar to the mean values of their genotypic group. **M–O:** Quantification of spine density and spine head volume based on 3D renderings. No difference in spine density was observed between genotypic groups (M), but an ~20% increase in average spine head volume was found for −/− layer 2/3 basal dendritic segments as compared with WT (N). The frequency distribution of spine head volumes reveals a rightward shift toward larger spines in −/− layer 2/3 basal dendritic segments (O). Scale bar = 4 μM for all images. **p ≤ 0.01, $^{\#}$p ≤ 0.1.

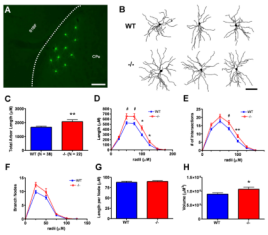

Figure 6.

Analysis of medium spiny neuron (MSN) morphometry in the dorsolateral caudate putamen (CPu) of postnatal day 40 wild type (WT) versus $Emx1^{cre}/Met^{fx/fx}$ (−/−) mice. **A:** Representative fluorescence micrograph of lucifer yellow immunoreactivity in microinjected medium spiny neurons in dorsolateral CPu in a coronal section. The dashed line represents the white matter boundary between striatum and overlying somatosensory barrel cortex (S1BF). **B:** Representative Neurolucida traces of MSNs. The neurons depicted have dendritic arbor morphometries approximate to the mean values of their genotypic group. **C–H:** Dendritic morphometry summary statistics. −/− MSNs exhibit an ~25% increase in total dendritic arbor length relative to their WT counterparts (C). Further analyses shows that increases in −/− dendritic length (D) and branching complexity (E) are distributed throughout the arbor and are likely due to an increase in the number of dendritic branches (F) rather than increased dendritic segment length *per se* (G). Three-dimensional convex hull analysis indicates an ~20% increase in −/− MSN arbor volume (H). Scale bar = 275 μM for A and 167 μM for B. $^{**}p \leq 0.01$, $^{*}p \leq 0.05$, $^{\#}p \leq 0.1$.

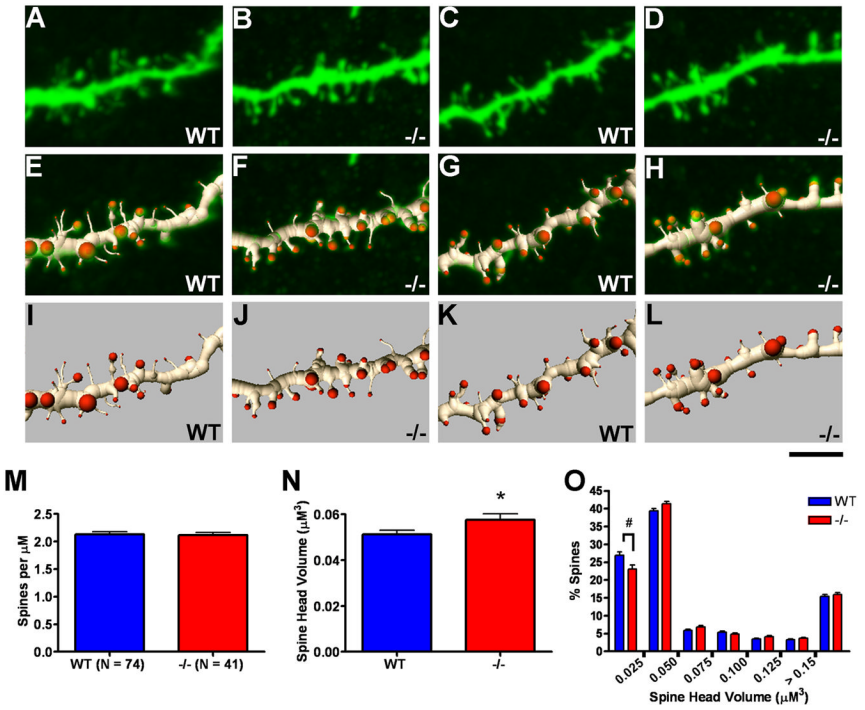

Figure 7.

Analysis of dendritic spines in postnatal day 40 wild type (WT) versus $Emx1^{cre}/Met^{fx/fx}$ (−/−) dorsolateral medium spiny neurons (MSNs). Confocal projection images of 2 WT (**A** and **C**) and 2 −/− (**B** and **D**) MSN dendritic segments (top row) and associated three-dimensional (3D) segmented renderings shown in overlay (middle row, **E,G** and **F,H**) and apart (bottom row, **I,K** and **J,L**). The images depict portions of analyzed full-length segments with spine density and spine head volume values similar to the mean values of their genotypic group. **M–O:** Quantification of spine density and spine head volume based on 3D renderings. No difference in spine density was observed between genotypic groups (M), but an ~12% increase in average spine head volume was found for −/−MSN dendritic segments as compared with WT (N). The frequency distribution of spine head volumes reveals a trend in −/− MSN dendrites toward decreased numbers of the thinnest spine types and significant increases in select classes of larger spines (O). Scale bar = 4 µM for all images. *$p \leq 0.05$, $^{\#}p \leq 0.1$.

Table 1

Primary Antibodies Used

Antigen	Immunogen	Manufacturer, Species, Catalog Number	Dilution Used
Met	Synthetic peptide, aa 1330–1379 of mouse C-terminus	Santa Cruz Biotechnology (Santa Cruz), mouse monoclonal (B-2), #sc-8057	1:500
Met	Synthetic peptide, aa 1228–1243 of human C-terminus	Cell Signaling Technology (Beverly), mouse monoclonal (25H2), #3127	NA
Phosphorylated Met	Synthetic KLH-coupled phosphopeptide ($Y^{1234}Y^{1235}$), aa 1228–1243 of human C- terminus	Cell Signaling Technology (Beverly), rabbit monoclonal (D26), #3077	1:1,000
Phosphorylated Tyrosine	KLH-coupled phosphotyramine	Millipore (Billerica), mouse monoclonal (4G10), #05-321	1:1,000
Lucifer Yellow	Dye-based hapten	Sigma (Saint Louis), rabbit polyclonal, #L9163	1:5,000

NA = not applicable